BAJOPMAS JOURNAL 16(2): 39 – 53
Printed in Bayero University, Kano - Nigeria.

MINERALS AND HYDROCARBON PROSPECT LOCATIONS MAPPING WITH REMOTE SENSING TECHNIQUES IN JIGAWA STATE, NIGERIA

[1]Magama, A.; [2]Aku, M. O. and [3]Saleh, M.
[1] Department of Physics, Sule Lamido University Kafin Hausa, Jigawa State. Nigeria.
[2,3] Department of Physics, Bayero University, Kano.
Corresponding Author: abdulhamida.magama@slu.edu.ng
Phone number: +2347030822780

ABSTRACT
Jigawa State is situated in Nigeria's northwest, between latitudes 11.00°N and 13.00°N and longitudes 8.00°E and 10.15°E. Despite having potential for hydrocarbons and valuable minerals, Jigawa is one of Nigeria's less explored states. This study uses multispectral image data from the LandSat-8 Operational Land Imager (OLI) and Advance Spaceborne Thermal Emission Reflection Radiometer (ASTER) to map alteration zones linked to valuable minerals. Prospective minerals and hydrocarbon alteration zones within the study area were mapped using a variety of remote sensing techniques, including Feature Oriented Principal Component Analysis (Crosta technique), Band Ratio, False Color Composite, Spectral Angle Mapper (SAM), Minimum Noise Fraction (MNF), Pixel Purity Index (PPI), Lineament, and Lineaments density analysis. Crosta technique, band ratio and false color composite results were able to map potential locations of ferric and ferrous irons, as well as carbonate minerals. The crosta technique results were able to identify areas of iron oxides and carbonate minerals. Using spectral analysis of endmembers spectra, SAM, MNF, and PPI classify three (3) distinct alteration zones (phyllic, propylitic, and argillic alterations). Four main trends were identified by lineament orientation analysis: NE-SW, E-W, NW-SE, and NNE-WSW. Lineament density map revealed four major areas with highest density located at east to extreme north-eastern corner trending from west to east, central parts, extreme north-west trending south to north and upper southern having the highest lineament density, the delineated alteration minerals coincide with areas of high lineament density. This research delineates areas of already existing mineral locations. Thus, this suggests the validity and reliability of the adopted methods used.

Keywords: Crosta, Hydrothermal alteration, Jigawa, Lineaments, Remote sensing, SAM.

1.0 INTRODUCTION
One important indicator of the potential occurrence of economic mineral deposits is the presence of altered rocks and sediments [1]. Because altered rocks and sediments have different reflectance spectra from unaltered ones, multispectral remote sensing can be used to identify them in areas where bedrocks and altered sediments are exposed [2]. Today, remote sensing and digital image processing allow us to use additional spectral bands for minerals and hydrocarbon exploration [3]. Understanding alteration zones and hydrocarbon seepage are essential for minerals and hydrocarbon exploration, as well as the evaluation of minerals and petroleum resources. Hydrothermal alteration and hydrocarbon seepage are two of the most significant features of minerals and hydrocarbon formation. Historically, the presence of minerals and hydrocarbon traps has been closely linked to the accumulation of hydrothermal alterations and hydrocarbon seepages [4]. As a result, many oil and gas fields across the globe have been drilled in macro and micro seeps locations. Macro seeps are

frequently viewed in contemporary exploration projects as clear indicators of source rocks and the development of strong proof of a petroleum system in each basin [5].

Hydrothermal alteration is any change in rocks or minerals brought about by a hydrothermal fluid reacting with previously formed solid phases [6]. Since hydrothermal alteration produces fingerprints that point to the location of desired mineral and hydrocarbon reserves, remote sensing has become widely used in the process of spectral identification of minerals [7]. A useful technique in mining prospection is the use of spectral signatures and spatial enhancements to locate hydrothermal alteration zones and structural features (lineaments). Numerous global studies [2]; [3]; [8]; [10]; [5]; and [11], among others) have been conducted to determine the zones where minerals form and to characterize the extent of hydrothermally altered areas using multispectral remotely sensed data.

Most of the geophysical works conducted in Jigawa State are based on mapping ground water potential. The most recent literature includes the works of [12], [13], [9], [14], and [15], among others. Very few geophysical and/or remote sensing researches regarding mineral and/or hydrocarbon investigation has been conducted in the study area, with a very scarce record of remote sensing work reported or documented within the available literatures. Few solid minerals have previously been found in some areas of the state by the Jigawa state investment and property development company limited and the state mineral resource development agency using geological techniques such as field mapping, direct visual observation, and sampling. It is obvious that the geologic method employed could not provide the optimum results needed for further investigation, as such, this may lead to the poor understanding of regional and local geology of the state.

However, the formation of kazaure Schist Belt (KZSB) which the Nigerian geological survey agency classify as undifferentiated schist (Figure 1), and the acclaimed existence of macro seepages presumably of petroleum origin at the vicinity of Birniwa, Kiri-kasamma, Sule Tankarkar and Babura local government areas of the state require significant attention to further investigate the KZSB and evaluate the genesis of the seepage, despite the aforementioned, there is neither available literature that supports these claims nor valid and comprehensive geophysical research that attempted to validate the genesis for further investigations. With the recent developments in the field of remote sensing, employing the use of multispectral remote sensing data could be key to understanding the regional and local geology of the state. Given that the majority of mining investigations are still in their early stages, this research could be of paramount importance to Jigawa State's mining industry. Hence, the need to bridge the unexplored gap through strategic geophysical investigation is important and of economic interest.

Based on the above mentioned, there is need to establish a substantive scientific fact on whether the macro-seepage mineralization emanate geochemically from hydrocarbon origin or not. Therefore, this research was done by processing and critically analyzing twenty-five (25) ASTER data scenes and six (6) Landsat-8 data scenes with the overall aim to providing crucial information on hydrothermally altered zones related to economic mineralization, and provide the needed data for further investigations in the state.

1.2 Location and Geology of the Study Area

Jigawa State is situated in Nigeria's northwest, between latitudes 11.00^{o}N and 13.00^{o}N and longitudes 8.00^{o}E and 10.15^{o}E (LAT 12° 26' 45.6", LONG 9° 43' 23.7612") covering an area of 23,154 km^{2} (8,940 square miles). The basement complex is located in Jigawa's southern region, and the Chad formation's sedimentary rocks are found in its northeastern parts.

Granites, schist, and gneisses of the basement complex underlie the northwest and southern regions of the state [9]. A hydrogeological divide that passes through the local governments of Yankwashi, Dutse, and Kiyawa separates the younger sediment of the Chad formation from the older Precambrian rocks of the basement complex [9].

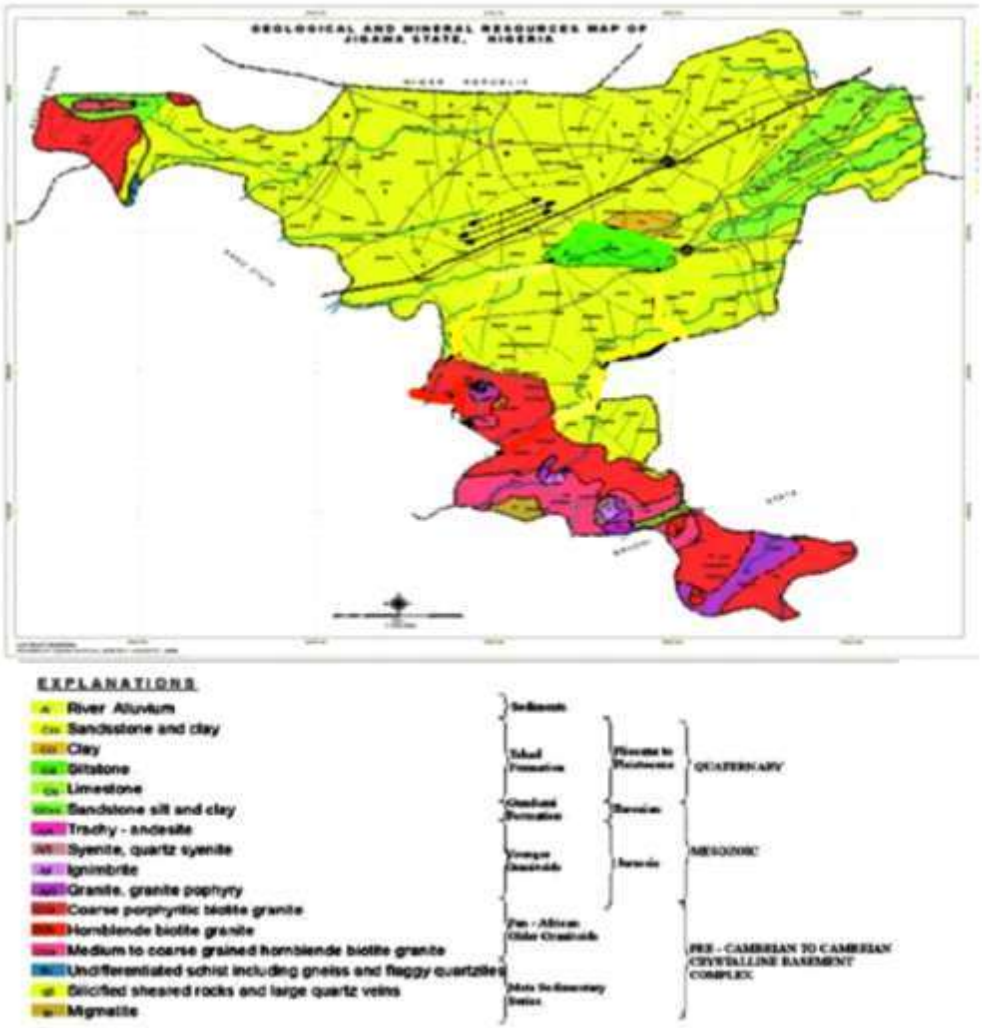

Figure 1: Geologic Map of the study area [14]

2.0 THEORETICAL BACKGROUND

In mineral and hydrocarbon exploration remote sensing aims to detect anomalies or patterns that may indicate the presence of mineral deposits or seepages. Spectral signature analysis is the means by which this is accomplished. In this section a brief explanation of the fundamental idea behind using satellite sensors for remote sensing to gather data from the Earth's surface is discussed.

2.1 Spectral Signature

Spectral reflectance, [ρ(λ)], serves as a function of wavelength and represents the relationship between incident and reflected energy. The tone and color of an object in a photograph are caused by spectral reflectance. The characteristic that allows an object or feature to be identified is its spectral signature, which is the average of its spectral

reflectance values over various, well-defined wavelength intervals. For a particular topographical feature, the spectral reflectance varies with wavelength. Spectral reflectance is a measure of the reflectance properties of features on the surface of the earth which is given by [16]:

$$\rho(\lambda) = \left[\frac{E_R(\lambda)}{E_I(\lambda)}\right] \text{ x } 100 \quad (1)$$

where;

$\rho(\lambda)$ = Spectral reflectance (reflectivity) at a particular wavelength
E_R = Energy of wavelength reflected from object
E_I = Energy of wavelength incident upon the object

3. MATERIALS AND METHODS

The materials used in this research includes LandSat-8 (OLI) data, ASTER data, ENVI v5.3 software, ArcMap v10.8 software, Geomatica Banff software, RockWorks20 software, Google Earth Pro software, Surfer21 software. These softwares were used to pre-process, process and interpret LandSat-8 and ASTER images. ENVI was employed in the pre-processing and processing of images. ArcMap was utilized for the generation and exportation of maps into different formats. Geomatica was utilized for automatic lineament extraction. RockWorks20 was used to generate lineament density map and rose diagram. Google Earth Pro was used to visualize location attributes. Whereas Surfer21was used for the insertion of shapes and word labels into the final image map.

3.1 Data Acquisition and Pre-Processing

The acquired data underwent the following pre-processing procedures: Radiometric calibration, FLAASH atmospheric correction, cross track illumination correction, layer stacking, rescaling and subset/clipping methods.

3.1.1 LandSat-8 (OLI) Data

The U.S. Geological Survey Earth Resources Observation and Science Center (USGS-EROS; http://earthexplorer.usgs.gov) provided cloud-free level 1T (terrain corrected) Landsat-8 OLI/TIRS sensor imagery (path 187, row 051), (path 187, row 052), (path 188, row 051), and (path 188, row 052) with 0% cloud cover, acquired on 13th March, 2023. The ENVI v5.3 was used to pre-process all four of the Level 1T standard terrain corrected image scenes. Eleven (11) bands makes up Landsat-8 OLI with five (5) Visible Near-Infrared (bands 1-5) having spectral range between 0.433 – 0.885μm, two (2) short wave infrared (bands 6 & 7) with spectral range between 1.560 – 2.300μm, band 8 (panchromatic band) having spectral range between 0.500 – 0.680μm, Band 9 (cirrus) ranging from 1.360 – 1.390μm and two (2) thermal infrareds (bands 10 & 11) having spectral range between 10.600 – 12.510μm.

LandSat-8 VNIR and SWIR bands were corrected using radiometric calibration tool, and subsequently transformed to surface reflectance in the Fast Line-in-sight Atmospheric Analysis Spectral Hypercube (FLAASH) to enable multitemporal stacking and multidate scene comparisons, the SWIR bands were also corrected using cross-track illumination correction tool of the ENVI software, the VNIR and SWIR bands were then layer-stacked. Radiometric and atmospheric corrections were applied to TIR bands using radiometric calibration and thermal atmospheric correction tool of the ENVI software. The VNIR and SWIR bands were layer stacked for subsequent processing, TIR bands were excluded for this specific research but, it was later been used for the detection of silicifications. The four

(4) LandSat-8 scenes were mosaicked using seamless mosaic tool, and then bilinearly resampled and subset to jigawa state using a shapefile.

3.1.2 ASTER Data

Aster data included 14 multispectral bands with three visible and near-infrared radiation bands (VNIR; 0.52 to 0.86 μm) with a spatial resolution of 15 m, six shortwave infrared radiation bands (SWIR; 1.6 to 2.43 μm) with a spatial resolution of 30 m, and five thermal infrared radiation bands (TIR; 8.125 to 11.65 μm) with a spatial resolution of 90 m. Twenty four (24) level 1T V3 cloud free ASTER scenes image data

(AST_L1T_00312212007100045_20150522110438_108032; AST_L1T_...102832; AST_L1T_...111437; AST_L1T_…110968; AST_L1T_…115750; AST_L1T_...94837; AST_L1T_...94839; AST_L1T_...67654; AST_L1T_...15323; AST_L1T_...15325; AST_L1T_...1401; AST_L1T_...1404; AST_L1T_87201; AST_L1T_...87203; AST_L1T_...69473; AST_L1T_...47242; AST_L1T_...82848; AST_L1T_...82843; AST_L1T_...18602; AST_L1T_...18602; AST_L1T_...93375, AST_L1T_...93384; AST_L1T_...94837; AST_L1T_...18602) of the study area were obtained from the U.S.G.S website (https://earthexplorer.usgs.gov). The ASTER scenes were obtained on 24th May 2023 and these images were subsequently georeferenced to the UTM zone 32North projection using the WGS-84 datum.

All the 14 ASTER bands were corrected using radiometric calibration tool and the cross-track illumination correction were applied to ASTER SWIR bands, the VNIR and SWIR bands were layer stacked and atmospherically corrected using FLAASH atmospheric correction by changing of the bands interleaves (BIL) tool of the ENVI, the radiometric and thermal atmospheric correction were separately applied to TIR bands and then subsequently layer-stacked with the VNIR and SWIR bands. Finally, the surface reflectance image was produced by rescaling the layer-stacked image for onward processing of the ASTER data. The twenty-four (24) ASTER scenes were mosaicked into one scene and spatially subset to region of interest (Jigawa state) using a shapefile in order to focus the investigation efforts to the study area.

3.2 Data Processing

3.2.1 Feature-Oriented Principal Component analysis (Crosta Technique)

The crosta technique was applied to the rescaled layer-stacked VNIR and SWIR bands of both ASTER and LandSat-8 data using forward PCA statistics and rotation tool of the ENVI software. After subsequent processing the statistical results of the obtained PCs eigenvector loadings were analyzed through visual inspection of the bands and principal components (PCs), the desired bands combination features were extracted and discriminated for iron oxides/hydroxide and carbonate/hydroxyl minerals mapping that are related to alteration minerals.

3.2.2 Band Ratios

The band ratio process was initiated by processing the results obtained from the PCs eigenvector loadings, this operation was performed by either band ratio or band math tools of the ENVI software. Using the band ratio interface of the ENVI software, the operational procedure involved designating a band with high reflectance for the mineral as the "numerator" and another band with high absorption as the "denominator."

3.2.3 False Colour Composite (FCC)

The FCC is achieved by combining bands in the visible and the near infrared portion, this is done in the data management interface of the ENVI software where the spectral bands information are displayed and the band colour combination are assigned.

3.2.4 Minimum Noise Fraction (MNF)

MNF reduces the number of data spectral dimensions. MNF image was produced using forward MNF estimate noise statistics tool. Some part of the endmember selection was done from the MNF data, spatial classification and selection was performed on MNF-FCC image. The analysis approach consists of spectral compression, noise suppression, and dimensionality reduction [17]. Higher eigenvalue images contain more spectral information because MNF component images exhibit a steadily declining image quality with an increase in band number [10]. Three MNF transformed bands with high eigenvalues were assigned to the Red, Green, Blue (RGB) color combination image.

3.2.5 Pixel Purity Index (PPI)

The higher-order MNF bands were selected for additional processing following MNF transformation. Using the Pixel Purity Index (PPI) function, the most spectrally pure pixels in multispectral data were found [8]. In order to identify the MNF image's most spectrally pure pixels, which usually correspond to an endmember, this research employ the use of PPI for dark pixel extraction in endmembers. As such, these pure pixels become the input for an interactive visualization process.

3.2.6 Spectral Angle Mapper (SAM)

Unsupervised and supervised SAM classification was performed on MNF generated images using spectral angle mapping classification algorithm tool, the first step was initiated by creating a spectral library through the extraction of spectral signatures within the selected region of interest (ROIs), those ROIs were extracted from the purest pixels of the MNF-PPI generated images. Endmembers were collected from varying locations of the isolated ROI pixels and then saved as the spectral library. SAM was then used to classify and map these spectra from the created spectral library [18] (Honarmand *et al.,* 2012). In order to identify alteration minerals, the acquired spectra were lastly compared with spectra from the USGS and John Hopkins spectral librararies.

3.2.7 Lineament Extraction

Using ENVI software, lineaments are extracted from Landsat-8's first principal component image (PC1). Given that PC1 contains the majority of the data and is appropriate for automatic line segment extraction. The Geomatica software's PCI-LINE module was utilized to extract lineaments. ArcGIS software was used to handle the extracted lineaments (splitting compound lines into simple lines, changing lineament attributes). Using the RockWorks20 software, the lineament output data were statistically analyzed to produce rose diagrams and assess variations in lineament direction and lineament density map.

4.0 RESULTS AND DISCUSSIONS

The results of the crosta technique, band ratio, false colour composite, minimum noise fraction, spectral angle mapper, lineaments, lineament density, and rose diagram are presented;

4.1 Feature-Oriented Principal Component Analysis (Crosta Technique)

Six bands of LandSat-8 OLI data were subjected to PCA (Table 1). Bands 1, 8, 9, and the TIR bands (10 and 11) were not included in the analysis. Only the VNIR and SWIR bands were used. This is because, our target minerals have no absorption or reflections within the excluded bands.

Table 1: Eigen Vector Loadings of Jigawa State for Mapping Iron Oxides/Hydroxides Minerals

LandSat-8 (OLI)					ASTER (VNIR + SWIR)				
PC1	**Band 2**	**Band 4**	**Band 5**	**Band 6**		**Band 3**	**Band 4**	**Band 5**	**Band 6**
PC2	-0.559419	-0.487814	-0.364163	-0.178844	**PC1**	-0.214105	-0.220637	-0.4090	-0.414921
PC3	**-0.344975**	-0.250668	0.162533	**0.649375**	**PC2**	**0.431273**	0.362116	0.58577	**-0.286220**
PC4	**-0.182465**	-0.079325	0.092882	**0.519284**	**PC3**	0.250449	0.157277	0.101833	0.157338
	-0.266188	-0.177524	0.868275	-0.371874	**PC4**	**0.591953**	0.373773	**-0.65956**	-0.167110

It could be seen that from Table 1(Landsat-8), band 6 has high positive loadings in PC2 (0.649375) and PC3 (0.519284) with PC2 having more strong loadings than PC3. Therefore, due to the strong positive loadings on band 6 (0.649375) and moderate negative loadings on band 2 (-0.344975), The iron oxide can be enhanced by PC2. On the other hand, PC3's band 6 (0.519284) and band 2 (-0.182465) have positive loadings that suggest the presence of hydroxyl-containing minerals as dark pixels. After careful examination of table 1, it could be observed that the ASTER band 3 has strong positive loadings (0.591953) and strong negative loadings of band 5 (-0.65956) in PC4.

Table 2: Eigen Vector Loadings of Jigawa State for Mapping Carbonate/Hydroxyls Minerals

LandSat-8 (OLI)					ASTER (VNIR + SWIR)				
PC1	**Band 2**	**Band 4**	**Band 5**	**Band 6**		**Band 3**	**Band 4**	**Band 5**	**Band 6**
PC2	-0.559419	-0.487814	-0.364163	-0.178844	**PC1**	-0.214105	-0.220637	-0.4090	-0.414921
PC3	-0.182465	-0.079325	0.092882	0.519284	**PC2**	**0.591953**	0.373773	**-0.659562**	-0.167110
PC4	-0.266188	-0.177524	0.868275	-0.371874	**PC3**	-0.101271	-0.041676	0.076830	0.710469
	0.630741	**-0.771902**	0.054433	0.049740	**PC4**	-0.124996	0.162841	-0.016302	0.150461

Moreover, there exist a medium to low positive loadings in band 3 (0.431273) and low negative loadings in band 6 (-0.286220) in PC2. Therefore, PC4 can be used to enhance iron oxides, while PC2 can be used to enhance hydroxides minerals within the study area. According to [19] one way to identify iron oxides alteration using crosta technique is by using Ferric/Ferrous Iron Index (FII), which is calculated as the ratio of reflectance values of 1.2μm to 0.9μm of Landsat images, FII can be used to detect the presence of iron oxides such as haematite, magmatite, and goethite which have characteristic absorption feature around 0.9μm. High FII values indicate the presence of iron oxides, while low FII values indicate their absence. Based on the FII in ASTER data, the spectral absorption features with 1.0–2.2μm and reflectance in 1.55–1.75μm found in iron oxides/hydroxides mineral groups correspond to ASTER band 4 (1.600 to 1.700μm) as described in 3.2.2. Consequently, ferric/ferrous mineral groups can be enhanced by PC2 of LanSat-8 and PC4 of ASTER.

[20], the spectral features of clay minerals and carbonates diagnostic are centered at 1.4μm, 1.75μm, 1.9μm, 2.20μm, and 2.35μm. Table 2 above represent the Spectral features of carbonates and clay minerals on LandSat-8 (OLI) and ASTER bands. The ASTER VNIR+SWIR dataset's eigenvector loading analysis reveals that PC2 has strong loadings of band 1 (0.591953) and band 5 (−0.659562) with opposite signs (Table 2). The clay minerals typically exhibit high reflectance in the 2.25–2.33μm range [20], these spectral ranges corresponds with band 4 and 5 of ASTER data as described in 3.2.2, and strong absorption characteristics in the 0.4–1.1μm range, which corresponds to bands 2, 3, and 4. Landsat-8 (OLI) eigenvector analysis reveals that PC4 has a strong positive loadings in band 2 (0.630741) and strong negative loadings in band 3 (-0.771902). it could be observed that

PC3 also has a strong positive and negative loading in bands 4 and 5 but, the observed spectral values exceed the spectral range for absorption and reflection of carbonate/hydroxyls minerals. As such, PC4 is much more suitable for enhancing carbonate/hydroxyls minerals within the study area.

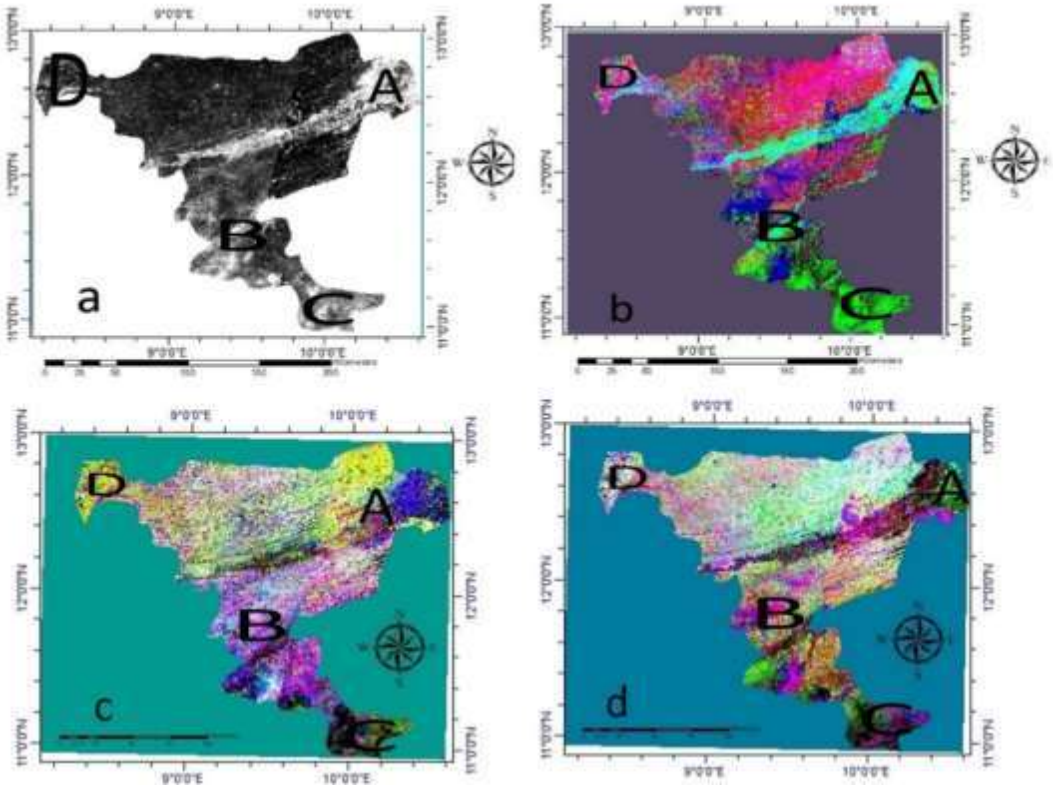

Figure 2: Landsat-8 False Colour Composite Maps. (a) Gray scale PC correlation matrix map (b) PC2 (R), PC3 (G), and PC4 (B) (c) Bands 753_RGB lithologic units (d) Bands 567 _RGB hydrothermal altered units

Thus, a Red, Green, and Blue (RGB) colour composite image of PC2 (R), PC3 (G), and PC4 (B) encompassing the study region is displayed in Figure 2 (b-d). Iron oxide/hydroxide minerals are shown in white gray colour as shown in Figure (2a) which reveals iron oxides/hydroxides minerals in white/grey colour that predominantly occupies northeast to western portions, central parts, southern parts and Extreme northwestern portion of the study area. Figure (2b) reveals iron oxides, carbonate and hydroxyls in red, green and dark & light blue pixels, portions (A & B) indicate the presence of iron and carbonate minerals, in particular portion (B) reveals the transition changes from ferric to ferrous oxides, the presence of iron oxide alteration surrounded by a carbonate minerals may indicate the presence of rocks intruded to the surface, portion (D) of the map reveals controlled alteration linearly pinkish colour trending from north to south. Figure (2c) reveals hydrothermal alteration along with the water bodies as demonstrated in white and scattered gray colours. Iron oxides, carbonate, and hydroxyls minerals are shown in blue, green, and pinkish pixels, indicating their presence in different lithologic units prevalent within the study area (see Figure 1 for comparisons). These minerals are mostly found in meta sediment, sand schists and sand stones [21].

4.1.2 Band Ratio

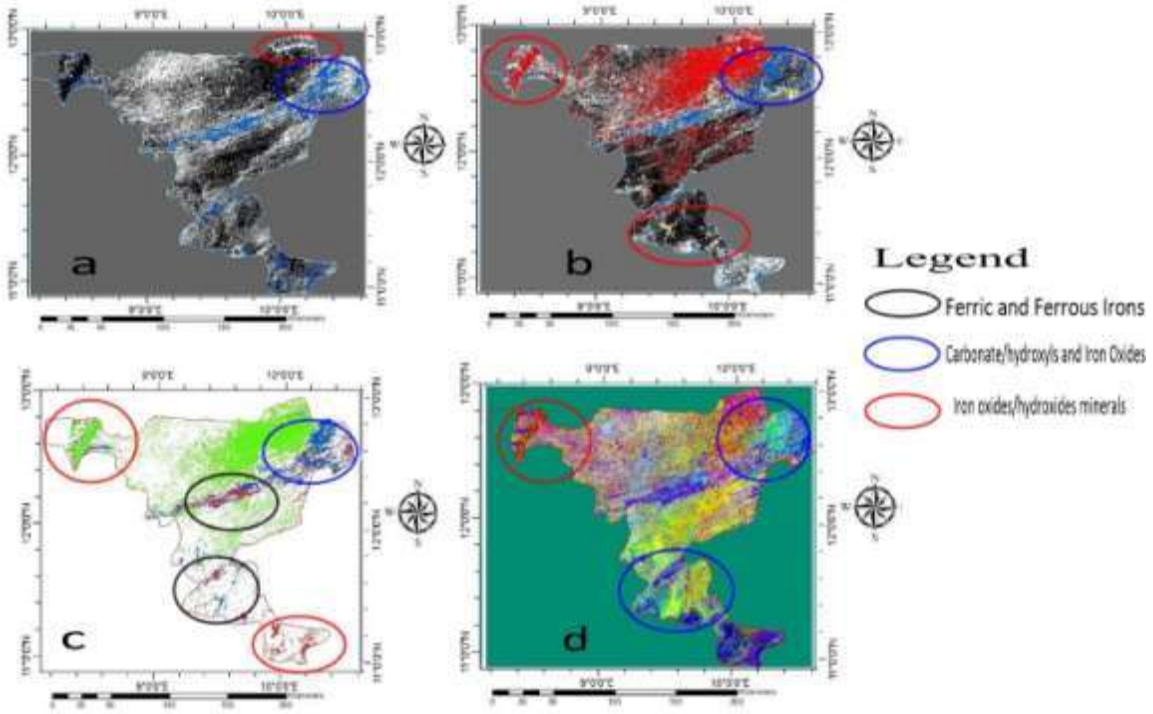

Figure 3: Band ratio classification. a) Crosta gray scale map superposed with clay/carbonate alteration b) Superposed band ratio alterations (4/2, 5/6, 6/7) c) Mapped hydrothermal alteration after applying the mask to the background features d) False colour composite of ratio (4/2, 5/6, 6/7).

Figure 3(a-d) reveals that northeastern parts such as Birniwa, Guri, Kirikasamma and some parts of Kafin hausa local governments (areas with blue circle) have promising hydrocarbon potentials due to the presence of ferric, ferrous irons and carbonate minerals and the presence of hydrothermally altered sediment coupled with the presence of high lineament density within the area. It could be seen that the northeastern parts of the state possess sediments enriched in ferric iron, hydroxyls and carbonate minerals which may likely undergo conversion from ferric to ferrous iron minerals, this is in line with the work of [22] (Shi *et al.,* 2010) were they inferred that the presence of hydrocarbon micro seepages are mostly associated with the conversion of ferric to ferrous irons within the seepage areas. As a result of these conversions, the sediments created by micro seepage lose ferric iron and develop bleaching. [1] Schumacher, (1996) mica and feldspars change into clay minerals due to the shifting oxidation-reduction conditions of the micro seepage environment. Thus, in soils and sediments impacted by micro seepage, clay minerals become abundant. As such, the Carbonate minerals are created when calcium or magnesium oxides in the sediments combine with carbon dioxide produced in the micro seepage environment [5] (Schumacher, 2010). However, northwestern and north-central (red and black circles) parts of the state show prospective formations of economic minerals due to the presence of hydrothermal altered rocks and sediments that has been revealed or intruded to the surface (Figure 1) within the area. It could be seen that most of the alteration minerals delineated within the area are structurally controlled from the surface indicating the presence of veins and/or schist belt areas.

4.1.3 Spectral Angle Mapper (SAM)

Supervised SAM classification technique was able to classify three (3) different hydrothermal alterations (Argillic, Phyllic and Propyllitic) within the vicinities of Birniwa, Guri, Kirikasamma, Kazaure, Dutse, Birnin kudu, Gwaram, Buji local government areas (Figure 4). Phyllic hydrothermal alteration were classified based on the examination of spectral signatures which the results of the examinations correspond to the spectral signatures of quartz, sericite and chlorite among others, based on the endmember spectra extracted from the regions of interest. The identification of argillic alteration was made possible due to the presence of illite, smicite, and kaolinite endmember minerals in the designated areas. Propylitic alterations were classified as endmember hydrothermal alteration due to the presence of epidote, chlorite, albite and calcite spectral signatures within the identified areas. The classification and mapping of the spatial distribution of common minerals in the alteration zones, including goethite, montmorillonite,

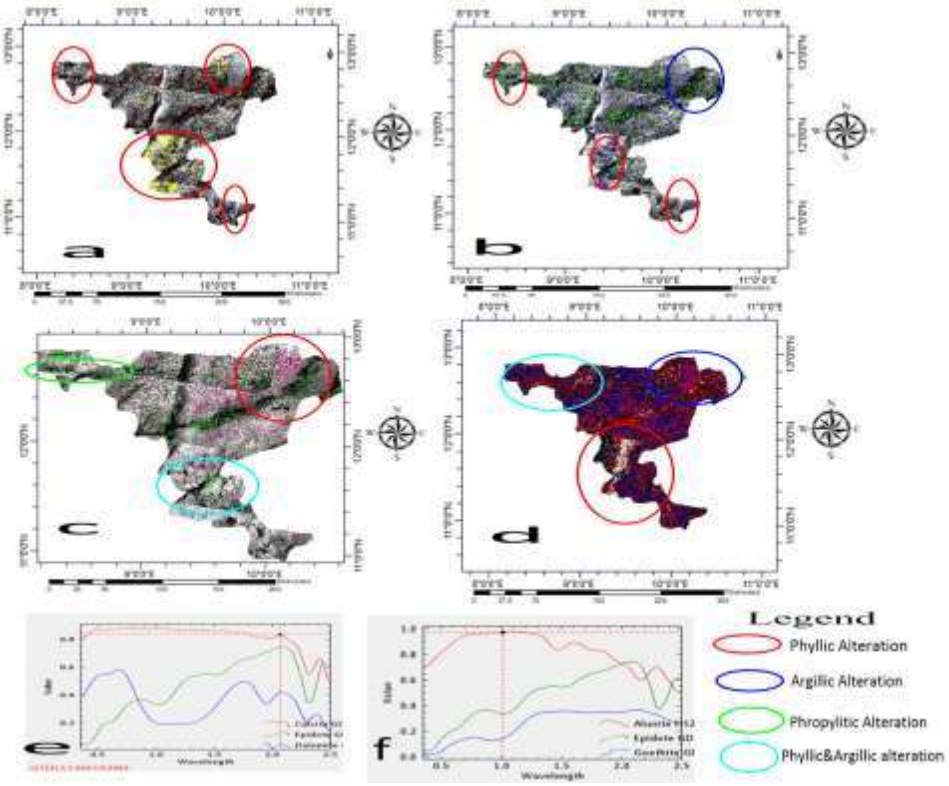

Figure 4: Aster Spectral Angle Mapper Classification a) Phyllic alteration; b) Argillic and phyllic alteration; c) Propylitic and phyllic alteration; d) Argillic and phyllic alteration; (e and f) Sample of spectral signature for three (3) important carbonate and hydrothermal alteration minerals build from USGS and USGS_ASTER spectral library.

Hematite, calcite, dolomite, illite, and chlorite, were done using spectral signature analysis and interpretations. Hematite which was used in the delineation of iron oxide minerals contains absorption features in bands 1 and 3 of ASTER. Calcite which was used in the classification of carbonate minerals shows absorption characteristics in bands 5, 6, and 7 with spectral reflectance peak at band 5 of ASTER. Dolomite exhibits spectral reflectance peak at band 2 of ASTER and weak absorption features in bands 3 and 4, with strong absorption features in band 6. Alunite exhibits distinctive absorption properties in bands 4 and 5 with spectral reflectance peak at band 3 of ASTER. Geothite has spectral absorption feature in band 4 and reflection in band 3 with spectral peak at band 5 (see Figure 4). Thus,

by applying the SAM classification algorithm, these spectral absorption and reflection signatures of alteration minerals in the VNIR+SWIR bands of ASTER were utilized to identify minute variations between alteration minerals.

4.1.4 Minimum Noise Fraction (MNF)

In order to interpret multispectral images from Landsat-8 data for geological and geophysical studies, a series of processing has to be performed. The color composite technique (Figure 4) produced an image that demonstrated a good level of alteration mapping. According to [17] and iron oxide minerals like hematite, goethite, and magnetite have high reflectance within 0.63 – 0.69μm and high absorption within 0.45 – 0.52μm. These characteristic features correspond to band 4 and 2 of landsat-8 as such, band ratio using band 2, and 4 were used to enhance iron oxide minerals, the same procedure was applied for enhancing carbonate minerals.

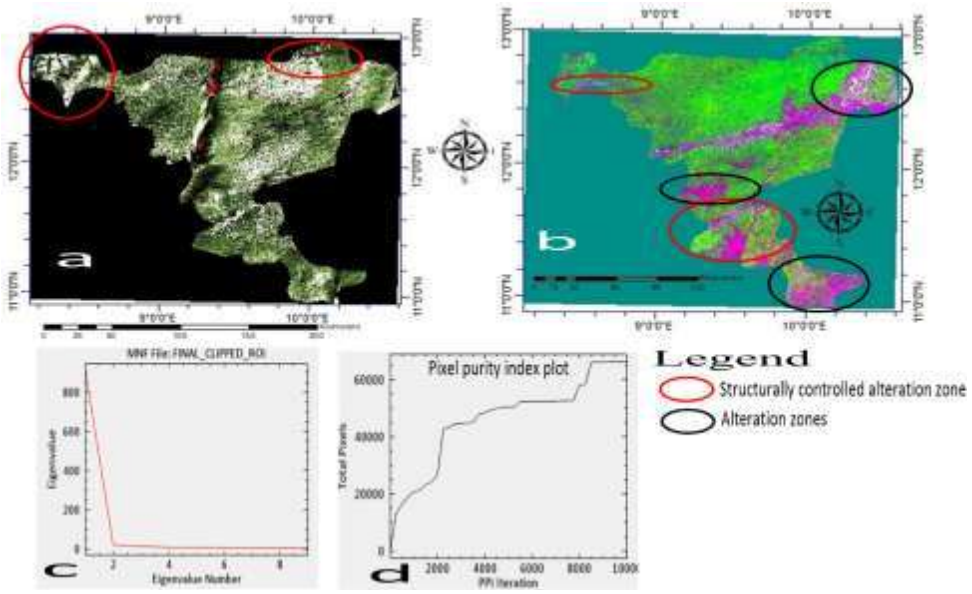

Figure 5: Minimum noise fraction map. (a) ASTER_MNF showing some structurally controlled alteration area (b) LandSat-8 FCC for the overall band ratios (c) Sample of ROI MNF plot (d) Pixel purity index plot.

According to [23] clay and carbonate minerals have reflectance from 1.55 – 1.75μm and absorption features from 2.1 – 2.4μm, these correspond to ASTER band 4, 6, and 9. Hence false colour combinations of these bands were subsequently used to enhance carbonate minerals. From the MNF transformed image (Figure 5a) the yellow and dark yellowish colours reveals areas iron oxides and carbonate minerals. Several linear alteration features both in yellow and dark yellow colours could be seen from the northwest, northeast, central, and Southern parts (Black circle) of the study area, this may be interpreted as surface controlled fractured areas due to the presence of high-density lineament and structurally surface controlled hydrothermal alterations, the upper portion of the northeastern part reveals similar pattern of unidentified surface alteration though the location has been characterized with the presence ferrous iron minerals related to phyllic alteration (Figure 5a and 5b). Figure 5b is the Landsat-8 FCC indicating overall alterations (4/2, 5/6, 6/7) by masking smaller features using dark pixel subtraction, pixel purity index and colour stretching techniques. the pinkish areas (Figure 5b) reveals structurally controlled alteration areas within the northcentral and northwestern parts (red circles), these areas exhibit significant lineament density and alteration features. Based on the results obtained FOPCA,

Band Ratioing, FCC, SAM and MNF, it could be said that these areas displayed the attractive features for the formation of economic minerals within the study area. Sample of MNF plot (figure 4.28) revealed band 2, 3, 4 as the most informative bands whereas bands 5, 6, and 8 exhibit data redundancy as the they all tends towards unity. As such bands 2, 3, and 4 which correspond to VNIR bands were selected for subsequent processing in that specific region of interest. Pixel purity index plot (Figure 4.29) total number of pixels plot against the PPI iterations, which shows a varying iteration based on the increase and decrease of the number of pixels which depends on the noise and purity of pixels in varying spatial locations.

4.1.4 Lineament Analysis

Lineament analysis is one of the intriguing methods in geological mapping and mineral exploration. Lineaments are discontinuities, either linear or curvilinear, that are directly related to faults and composite fractures [24] (Thannoun, 2018). In this research automatic lineament extraction were adopted because it is fast, reliable, less ambiguous and non-subjective. Four orientations were identified within the subgrouping of lineaments: NE-SW, E-W, NW-SE, and NNE-WSW.

The N60^{o}E to N70^{o}E and S250^{o}W to S240^{o}W are the predominant lineament direction within the study area, this agrees well with the work of [12] (Ibrahim & Musa, 2020), and [15] (Danbatta, 2010). The second predominant lineaments directions are N70^{o}E to N80^{o}E and S260^{o}W to S270^{o}W. The N50^{o}E to N60^{o}E, N80^{o}E to N90^{o}E, S270^{o}W to S260^{o}W and S240^{o}W to S250^{o}W are the NE-SW directions within the study area that correspond to the average direction of all detected lineaments. The minor lineaments trends within the study area dwell within the orientations S100^{o}E to S110^{o}E, N10^{o}E to N20^{o}E, N280^{o}E to N290^{o}E, and S220^{o}W to S230^{o}W. The results of the lineament analysis conducted in this research revealed that NE, NNE, SW and WSW are the dominant lineaments (structural trend) while NNW, NW, SE, and SSW are the minor structural trends within the study area.

The Jigawa state lineament density map (figure 6) reveals varying strength of lineament density, areas with brown and yellow colours signify locations with the highest lineament density strength, green colour indicates areas with moderate density whereas pink colour indicate areas with medium to low lineament density. The obtained lineament trends extracted from the study area reveals zones of high, moderate and low structural lineament density trending NE, NW, WNW, SW, and SE directions.

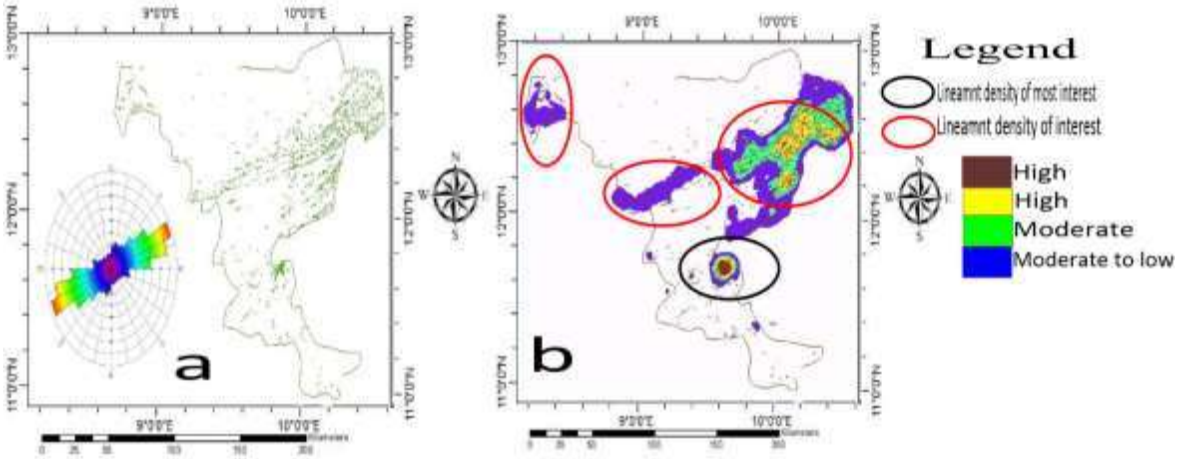

Figure 6: Lineament Map. a) Lineament with rose diagram b) Lineament density map.

5.1 CONCLUSION

Based on the results obtained, this research delineates locations of minerals prospective zones in Jigawa NorthWest (Kazaure, Gora, Gawuna, Manad, Dutsin wahla, Roni, Dutsin kodawa, Dansure, Nanumawa, Tsubut, Farartukwane, Gwiwa, Koreyel, Malaganta, Shafe, Tinkishi, Wuntsila, Kuzunzunmi, Garin gudiniya, Yanzaki and Tsadoji). Central and Southern Jigawa (Dutse, Buji, Birnin Kudu, Gwaram, Isawa, Gogura, Kafin filani, Kila, Zandam, Kafin doki, Galala, Samamiya, Mafudi, Gingino, Jallawa, Shafada, Zumburum and Baram and hydrocarbon prospective zones in Jigawa NorthEast (Guri, Gogiya, Birniwa, Kirikassama, Jerau, Marma, Gaduwa, Abinabo, Chachamau, Musari, Takara, Tazga, Sugum, Dagilfani, Dajin Bula, Matafari, Kuka uku, kukawa, Kakori, Tukwiki and Matara gabas). Results obtained from FOPCA (crosta technique) were able to delineate areas of iron oxides and carbonate minerals, band ratio and false colour composite were able to map prospective locations ferric and ferrous oxides minerals, and carbonate minerals in addition to that of crosta technique. SAM, MNF and PPI classified three (3) different alteration zones (Argillic, phyllic, and propylitic alterations) using spectral analysis of endmembers spectra. Lineament orientation analysis revealed four major trends NE-SW, E-W, NW-SE and NNE-WSW. Lineament density map revealed three major areas with highest density located at the extreme north-eastern part trending west, central parts and extreme north-western of part of the study area, the delineated alteration minerals coincided with high lineament density. The result obtained from this research delineated areas of already existing economic mineral locations. Thus, this suggests the reliability and validity of the methods been adopted and used. The study also revealed new prospective locations for further hydrocarbon and mineral exploration. It is suggested that further geophysical research such as gravity, magnetics, resistivity, induced polarization, ground penetrating radar, magnetelluric, geochemical, seismic reflection and refractions methods should be conducted within the identified prospective regions.

REFERENCES

[1] Schumacher, D. (1996). Hydrocarbon-induced alteration of soils and sediments. *AAPG Memoir*, *66*, 71–89. https://doi.org/10.1306/m66606c6

[2] Ousmanou, S., Fozing, E. M., Kwékam, M., Fodoue, Y., & Jeatsa, L. D. A. (2023). Application of remote sensing techniques in lithological and mineral exploration: discrimination of granitoids bearing iron and corundum deposits in southeastern Banyo, Adamawa region-Cameroon. *Earth Science Informatics*, *16*(1), 259–285. https://doi.org/10.1007/s12145-023-00937-5.

[3] Rebouh, N., Oudni, A., Khiari, A., Benabbas, C., & Özgür, N. (2021). Hydrothermal alteration mapping and structural features in the Ain Smara basin, Constantine (Northeastern Algeria): contribution of Landsat OLI8 data. *Arabian Journal of Geosciences*, *14*(21). https://doi.org/10.1007/s12517-021-08487-0.

[4] Sekandari, M., Masoumi, I., Pour, A. B., Muslim, A. M., Rahmani, O., Hashim, M., Zoheir, B., Pradhan, B., Misra, A., & Aminpour, S. M. (2020). Application of Landsat-8, Sentinel-2, ASTER and Worldview-3 spectral imagery for exploration of carbonate-hosted Pb-Zn deposits in the Central Iranian Terrane (CIT). *Remote Sensing*, *12*(8). https://doi.org/10.3390/RS12081239.

[5] Schumacher, D. (2010). *Integrating Hydrocarbon Microseepage Data with seismic Data Doubles Exploration Success*. *May 2010*. https://doi.org/10.29118/ipa.1277.10.g.104

[6] Huntington, J. F. (1996). The role of remote sensing in finding hydrothermal mineral deposits on earth. *CIBA Foundation Symposia*, *202*, 214–235. https://doi.org/10.1002/9780470514986.ch12.

[7] Mahboob, M. A., Genc, B., Celik, T., Ali, S., & Atif, I. (2019). Mapping hydrothermal minerals using remotely sensed reflectance spectroscopy data from Landsat. *Journal*

of the Southern African Institute of Mining and Metallurgy, *119*(3), 279–289. https://doi.org/10.17159/2411-9717/2019/v119n3a7

[8] Zamyad, M., Afzal, P., Pourkermani, M., Nouri, R., & Jafari, M. R. (2019). Determination of Hydrothermal Alteration Zones Using Remote Sensing Methods in Tirka Area, Toroud, NE Iran. *Journal of the Indian Society of Remote Sensing*, *47*(11), 1817–1830. https://doi.org/10.1007/s12524-019-01032-3

[9] Adamu, S. B., Idris, M. C., & Ibrahim, G. S. (2018). Geo-Electric Investigation of Aquifer Characteristics and Ground Water Potential in Kafin Hausa, Jigawa State, Nigeria. *Dutse Journal of Pure and Applied Sciences*, *4*(2), 434–443.

[10] Luo, G., Chen, G., Tian, L., Qin, K., & Qian, S. E. (2016). Minimum Noise Fraction versus Principal Component Analysis as a Preprocessing Step for Hyperspectral Imagery Denoising. *Canadian Journal of Remote Sensing*, *42*(2), 106–116. https://doi.org/10.1080/07038992.2016.1160772

[11] Sabins, F. F. (1999). Remote sensing for mineral exploration. *Ore Geology Reviews*, *14*(3–4), 157–183. https://doi.org/10.1016/S0169-1368(99)00007-4

[12] Ibrahim, A., & Musa, A. (2020). Mapping geology and structural features of Kazaure SE, NW Nigeria: Justifying groundwater potential model. *Zbornik Radova Departmana Za Geografiju, Turizam i Hotelijerstvo*, *9*(49–1), 1–21. https://doi.org/10.5937/zbdght2001001k

[13] Ndikilar, C. E., Idi, B. Y., Terhemba, B. S., Idowu, I. I., & Abdullahi, S. S. (2019). Applications of Aeromagnetic and Electrical Resistivity Data for Mapping Spatial Distribution of Groundwater Potentials of Dutse, Jigawa State, Nigeria. *Modern Applied Science*, *13*(2), 11–28. https://doi.org/10.5539/mas.v13n2p11

[14] Hamidu, H., Falalu, B. H., Abdullahi, I. M., Kwaya, M. Y., & Arabi, A. S. (2017). Groundwater chemistry, storage and dynamics in parts of Jigawa Central, Northwestern Nigeria. *Bayero Journal of Pure and Applied Sciences*, *10*(1), 138. https://doi.org/10.4314/bajopas.v10i1.19

[15] Danbatta, U. A. (2010). On the evolution of the Kazaure Schist Belt of NW Nigeria: a re-interpretation. *Global Journal of Geological Sciences*, *8*(2), 207–216. https://doi.org/10.4314/gjgs.v8i2.62775

[16] Aggarwal, S. (2013). *Principles of Remote Sensing*. University Press. Pp. 28-29.

[17] Joseph, A. and Bamidele, O. (2018). Application of Remote Sensing Method for Geological Interpretation of Sokoto Plain, Nigeria. *South African Journal of Geomatics, 7*(3), 360 – 371. *http://dx.doi.org/10.4314/sajg.v7i3.12*

[18] Honarmand, M., Ranjbar, H., & Shahabpour, J. (2012). Application of Principal Component Analysis and Spectral Angle Mapper in the Mapping of Hydrothermal Alteration in the Jebal-Barez Area, Southeastern Iran. *Resource Geology*, *62*(2), 119–139. https://doi.org/10.1111/j.1751-3928.2012.00184.x

[19] Loughlin, W. P. (1991). Principal Component Analysis for Alteration Mapping. *Photogrammetric Engineering & Remote Sensing, 57*(9), 1163 – 1169.

[20] Zhang, G., Shao, Z., & Huang, Y. (2013). *Hydrocarbon-induced clay and carbonate minerals interpretation in Songliao Basin using ASTER data*. www.earthexplorer.usgs.gov

[21] Huang, S., Chen, S. B., & Zhang, Y. Z. (2019). Comparison of altered mineral information extracted from ETM+, ASTER and Hyperion data in Águas Claras iron ore, Brazil, North America. *IET Image Processing*, *13*(2), 355–364. https://doi.org/10.1049/iet-ipr.2018.5026

[22] Shi, P., Fu, B., & Ninomiya, Y. (2010). Mapping hydrocarbon seepage-induced anomalies in the arid region, west China using multispectral remote sensing. *International Archives of the Photogrammetry, Remote Sensing and Spatial Information Sciences - ISPRS Archives*, *38*, 442–447.

[23] Garain, S., Mitra, D., and Das, P., (2021). Mapping hydrocarbon microseepage prospect areas by integrated studies of ASTER processing, geochemistry and geophysical surveys in Assam-Arakan Fold Belt, NE India. *International Journal of Applied Earth Observations and Geoinformation, 102*(2021), 1 – 18.

[24] Thannoun, R. G. (2018). *Automatic Extraction and Geospatial Analysis of Lineaments and their Tectonic Significance in some areas of Northern Iraq using Remote Sensing Techniques and GIS*. *November*. https://doi.org/10.13140/RG.2.2.20851.99363